Germanene and stanene on two-dimensional substrates: Dirac cone and Z_2 invariant

Zeyuan Ni,[1,*] Emi Minamitani,[1] Yasunobu Ando,[2] and Satoshi Watanabe[1]

[1]*Department of Materials Engineering, The University of Tokyo, Tokyo 113-8656, Japan*
[2]*Research Center for Computational Design of Advanced Functional Materials, The National Institute
of Advanced Industrial Science and Technology (AIST), Tsukuba, Ibaraki 305-8568, Japan*

By using the combination of the *ab initio* density functional theory and data mining of the Inorganic Crystal Structure Database, a series of monolayer materials are found to be suitable substrates for germanene or stanene, including some of the CdI$_2$-type materials, CuI, and GaGeTe. All of the found materials, when they are used as the substrate, can almost preserve the quasifreestanding geometry, stability, and band structure of germanene or stanene. Among them, CdI$_2$ and ZnI$_2$ can open a relatively large band gap of 0.16–0.18 (0.13–0.16) eV [without (with) spin-orbit coupling] in germanene, while preserving Dirac-cone-like band structures. Moreover, the Z_2 invariants of germanene on CuI and stanene on CaI$_2$ are found to be nontrivial. The interaction between germanene and substrates can be well modeled by the low-energy tight-binding Hamiltonian of germanene under external fields. Our analysis based on the tight-binding Hamiltonian shows that suitable substrates mainly act like a "pseudoelectric" field on germanene, and that strong linear correlations are seen among the "pseudoelectric" field, extrinsic Rashba coefficient, and charge transfer.

I. INTRODUCTION

Graphene and its various fascinating properties, including the massless Dirac fermions and the nontrivial topological state, have stimulated numerous scientific breakthroughs [1,2]. However, the zero-gap nature and the small spin-orbit coupling (SOC) in graphene largely hinder its application [1], which motivates the search for two-dimensional (2D) materials beyond graphene [3]. Germanene and stanene [4], as the Ge and Sn analogs of silicene and graphene, naturally become two of the candidates. In theory, similar to graphene and silicene, freestanding germanene and stanene also have the Dirac cone in their band structures [5], bringing them ultrahigh carrier mobility and quantum spin Hall effect (QSHE) as 2D topological insulators [2,6,7]. They also can be used to fabricate vertical transistors based on Dirac materials [8]. Beyond the similarity, germanene and stanene have stronger SOC and larger SOC gaps of over 23 and 73 meV [6,7,9,10], respectively, compared to 1.55 meV in silicene and 8 μeV in graphene [9,11], leading to the possibility of room-temperature 2D topological insulators [12,13]. Their buckled structures make their band structures even more tunable than monolayer graphene by external electric field or surface atom adsorption [14–18]. Moreover, germanene is predicted to have doubled intrinsic carrier mobility, one order of magnitude smaller electron-phonon coupling, and three times longer spin dephasing length compared to graphene [19–21]. In experiment, germanene has been synthesized on various kinds of substrates [22], including Pt(111) [23,24], Au(111) [25], Ge$_2$Pt [26,27], and Al(111) [28], and stanene has been synthesized on a Bi$_2$Te$_3$ surface [29]. Very recently, germanene was synthesized on MoS$_2$ [30], which is the first time that a 2D semiconducting substrate was used for germanene in experiment. Although germanene becomes semimetallic in experiment due to strain [30], theoretical research predicts

that germanene can keep its nontrivial topological state on MoS$_2$ [31].

However, two problems remain to be solved: (1) Germanene and stanene still lack suitable semiconducting substrates. In experiment, most of the reported substrates are metallic, except for MoS$_2$. On those metallic substrates, researchers fail to observe solid evidence of the Dirac cone in germanene and stanene. Even for germanene on MoS$_2$, the existence of the hole pocket at the Γ point induced by the $\sim$5% strain renders the utilization of the Dirac cone properties at the K point difficult [30]. Stanene on MoS$_2$ was also investigated theoretically very recently, but there is still controversy over whether stanene can remain semiconducting or will become semimetallic [32,33]. Unfortunately, traditional insulating or semiconducting substrates such as bare SiO$_2$ and GaAs strongly interact with germanene and ruin the Dirac cone [14,34]. Some of the hydrogen-passivated surfaces have been predicted to be promising to preserve the properties of germanene and its cousin materials: for example, H-passivated Si(111) and Ge(111) surfaces for silicene [35], H-passivated GaAs(0001) surface for germanene [34], and H-passivated SiC(0001) for stanene [36]. Stanene is also predicted to be able to preserve the nontrivial topological phase on the α-Al$_2$O$_3$ (0001) surface [37]. Nevertheless, substrates that do not require additional treatment and have small lattice mismatch remain to be investigated systematically. (2) Germanene and stanene should be supported or protected by solid substrates in practice, but the effect of substrate on the electronic state and Z_2 topological indexes of supported germanene and stanene remain to be investigated systematically. Currently, the Z_2 invariant of germanene on MoS$_2$, and h-BN, and that of stanene on InSe, GaTe, Ge(111), and H-passivated SiC have been studied [10,31,36,38,39]. Recently, Matthes *et al.* investigated the topological state and the frequency-dependent spin Hall conductivity of germanene and halogenated germanene [40,41]. Whether germanene and stanene have different topological phases on other substrates and how to explain the interaction between

---

*zeyuan_ni@cello.t.u-tokyo.ac.jp

germanene/stanene and 2D substrates in general are still open questions.

Using 2D layers from three-dimensional (3D) layered materials as the substrate can be a possible solution to the first problem and has several advantages. Three-dimensional layered materials have weaker interaction between each layer compared to three-dimensional materials, which may help in protecting the structural integrity of germanene and stanene. Two-dimensional substrates from 3D layered materials can also be directly used in the fabrication of the vertical layer-by-layer heterostructure and vertical field effect transistor [42,43]. Moreover, besides the potential as substrates, 2D layers can also act as protective films to prevent germanene and stanene from being degraded in the ambient environment [22]. Previously our group and another group had proposed that 2D GaTe and InSe can be potentially suitable substrates for germanene and stanene, respectively [38,44]. Nevertheless, such human selection of substrate candidates by experience, both in experimental and theoretical studies, is of less efficiency.

In this work, by using density functional theory (DFT) and materials informatics, we have dug out several suitable 2D semiconducting substrates for germanene and stanene, including some of the CdI_2-type materials, GeI_2, CuI, and GaGeTe, from the Inorganic Crystal Structure Database (ICSD) [45]. After mining and screening by our homemade program, the structural and electronic behaviors of monolayer germanene/stanene on the selected candidate substrates are investigated by using DFT. On these suitable substrates, germanene and stanene are found to be able to preserve quasifreestanding geometries and Dirac-cone-like band structures with band gaps of 0.004–0.157 eV [with spin-orbit coupling]. The stability of the supported germanene and stanene is examined by phonon calculations. In addition, we have performed systematic investigation on the Z_2 topological index of the supported germanene and stanene, and have found that they can even preserve their nontrivial Z_2 topological index on CuI and CaI_2, respectively. On the other substrates, germanene and stanene become trivial band insulators, even though the interaction with substrates are van der Waals–like. Furthermore, we have demonstrated that the interaction between germanene/stanene and the substrates can be well explained by the low-energy Hamiltonian of freestanding germanene/stanene under uniform external fields.

II. METHOD

We use our homemade program to filter out such materials from ICSD and get the structure data [46]. In this work, we aim at providing several suitable substrates within reasonable computational costs, so we focus on the layered substrates that can have 1×1 stacking configuration with germanene and stanene. On the basis of the experience gained from our previous study, we select the substrates using the following criteria:

(1) They shall be stable in experiment at room temperature and atmospheric pressure.

(2) They shall have small lattice mismatch (<6%) to germanene or stanene.

(3) They shall have symmetry similar to the host material (hexagonal lattice in this case).

(4) They shall not contain heavy elements and magnetic elements, namely Co, Cr, Fe, Mn, Mo, Ni, V, W, and La-Ac series elements. This criterion is added to simplify the automatic DFT calculation procedure in the later step. Heavy elements and magnetic elements sometimes require case-by-case treatment like DFT + U and correct initial guess of magnetism.

(5) They shall be 2D materials or 3D layered materials.

The above criteria can be easily extended in order to take into account substrate candidates that may form a larger rotated commensurate lattice, with one example given in the Discussion section.

Inspired by the idea of data mining of 2D materials in ICSD [47], we use our homemade program to filter out suitable 2D substrate candidates from ICSD for germanene and stanene. We use an interlayer distance criterion of 3.0 Å to select those materials with large vacuum in the z direction. The above criterion is selected in consideration of the interlayer distance of graphene and the balance between computation time and the success rate in searching for finally suitable substrates (for details, see the Supplemental Material [48]). The candidate for suitable substrate derived by the above algorithm is doubly checked by another algorithm: First, we make the bonding check between all atom pairs in the material to build a connection table. The bonding check is made by comparison of the distance between two atoms and the sum of the covalent radii of the elements from the database in *Mathematica* times 1.33 (an empirical coefficient to count all ambiguous interatomic distances as connected); then we separate the atoms into groups based on whether they are connected or not and determine the dimensionality by the comparison between the number of groups in the primitive cell and the $2 \times 2 \times 2$ super cell. The bulk structures of the suitable substrates found in this work are shown in Fig. S1 [48]. After selection, the DFT method implemented in QUANTUM ESPRESSO is used to examine the performance of germanene and stanene on their corresponding substrate candidates [49], and a homemade program is used for the automation of extensive DFT calculations. Projector augmented wave (PAW) pseudopotentials from PSlibrary are employed in geometry optimization, band structure, and phonon dispersion calculations [50,51]. For each element, we select the pseudopotential with the highest suggested energy cutoff and use such cutoff in our calculation. The optB86b-vdW exchange-correlation functional is used in geometry optimization to take the van der Waals (vdW) interaction into account [52–55]. The generalized gradient approximation (GGA) exchange-correlation functional of the Perdew, Burke, and Ernzerhof (PBE) parametrization is utilized in electronic structure calculations with SOC [56]. A Monkhorst-Pack (MP) k-point grid of $21 \times 21 \times 1$ is chosen for all systems after testing [57], since our target systems have similar lattice constants. The energy and force convergence tolerance are set to 1×10^{-5} Ry and 2×10^{-4} Ry/Å, respectively. We do not perform variable-cell optimization, so the pressure convergence is not necessary. Dipole correction is applied and found to have negligible influence in our systems [58]. Phonon calculations are performed by using density functional perturbation theory (DFPT) implemented in QUANTUM ESPRESSO
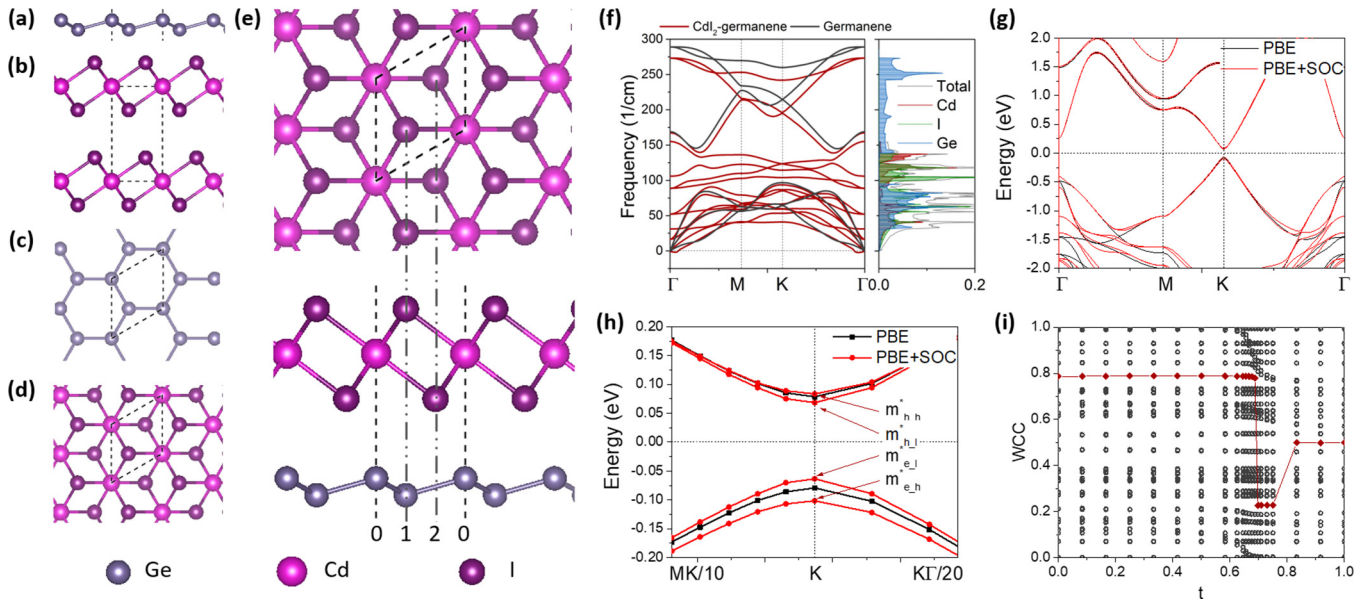
FIG. 1. (a–d) Top and side view of freestanding germanene and one kind of substrate, a type of bulk CdI$_2$ (ICSD ID: 6066). (e) Top and side view of the most preferable geometry of germanene on monolayer CdI$_2$. The numbers at the bottom ("0210") denote the high-symmetric points in the hexagonal cell. (f) Phonon dispersion (left) and phonon partial density of states (PDOS, right) of the germanene-CdI$_2$ system. The phonon dispersion of freestanding germanene is also given as gray lines in the left figure. (g) Band structure of the germanene-CdI$_2$ system. (h) Band structure of the germanene-CdI$_2$ system adjacent to the K point in the reciprocal space. The SOC introduces splits in the valence band and conduction band, so there are four effective masses in germanene. (i) Evolution of Wannier charge center (WCC) over time t (k_y in 2D case) used for the calculation of the Z_2 invariant. Gray hollow circles are the positions of WCCs, and the red diamonds mark the center of the largest WCC gap.

with a q-point grid of $5 \times 5 \times 1$ [49]. Norm-conserving pseudopotentials generated by optimized norm-conserving Vanderbilt pseudopotential (ONCVPSP) using the SG15 data set are employed in Z_2 invariant calculations implemented in Z2PACK supported by WANNIER90 after testing [48,59–63].

To illustrate the research routine applied to each substrate candidate, let us take CdI$_2$, a typical substrate candidate for germanene, as an example. One type of bulk CdI$_2$ [Figs. 1(b) and 1(d), ICSD: 6066] has a hexagonal lattice with a lattice constant of 4.24 Å. The lattice constant is similar to that of the freestanding germanene [4.02 Å, Figs. 1(a) and 1(c)], so we adopt a 1×1 stacking configuration [Fig. 1(e)] for the germanene-CdI$_2$ system. Such 1×1 configuration is applied to all other cases for the same reason. A monolayer substrate is chosen to reduce the overall computational cost and generally should yield results similar to the corresponding bulk substrate according to our previous study [44], because all candidates have layered structures. In order to search for the most energetically favorable geometry, first a randomly stacked germanene-CdI$_2$ system is optimized at different lattice constants (Fig. S2 [48]) to obtain the optimal cell size. Then the most stable stacking pattern of germanene on CdI$_2$ is investigated. Because there are three high-symmetric points [marked as 0, 1, and 2 below the dashed lines in Fig. 1(e)] in one hexagonal cell and two different Ge atoms in germanene, there are $\binom{3}{2} = 6$ high-symmetric stacking patterns in total. The six stacking patterns are labeled as Ge^{i}Ge^{j}I^{k}Cd^{l}I^m, where i, j, k, l, $m = 0$, 1, 2 denoting the high-symmetric points. Other non-high-symmetric stacking patterns are found to be less preferable in our previous research

of similar systems and thus are ignored in this work [44]. The most stable stacking pattern is found to be Ge^{1}Ge^{0}I^{2}Cd^{0}I^1 [Fig. 1(e), Fig. S3] [48], which is characterized by an AB-like tip-to-valley configuration with the highest atoms ("tips") in bulked germanene and CdI$_2$ aligned to the hollow centers ("valleys") in each other like a pair of gears. Such a tip-to-valley configuration results in a significantly smaller interlayer distance between germanene and CdI$_2$ compared to the other tip-to-tip configurations (Fig. S3 [48]), leading to a smaller total energy. Nevertheless, the interlayer distance is still as large as ~3.2 Å, suggesting the weak interaction between the two materials. Note that although there is another tip-to-valley configuration named Ge^{0}Ge^{1}I^{2}Cd^{0}I^1, which is only 0.01 eV over the most stable one, the two tip-to-valley configurations are related by a space inversion operation instead of any lateral translation of the germanene part and thus actually have a much higher energy barrier between them according to our previous research [44].

The stability of the germanene-CdI$_2$ system is established by phonon calculations. Its phonon dispersion, shown in Fig. 1(f), is all positive except for small ($<2\,\text{cm}^{-1}$) negative frequencies near the Γ point. The negative frequency is supposed to be a part of the out-of-plane acoustic (ZA) branch of germanene and can be also found in freestanding germanene [5]. Such minor negative frequency pocket can be eliminated [64,65], for example, by improving the optimization accuracy [gray lines in Fig. 1(f) by this group]. As a result, we believe that it does not affect the stability of the system and do not further optimize the phonon calculations due to the lack of computational resource and significance.

TABLE I. Structural properties, including the lattice constant of bulk substrate (a_{sub}) and system of monolayer substrate with germanene/stanene (a_{sys}), final lattice mismatch a_{mis} between the system and freestanding germanene/stanene, stacking pattern, buckling Δ, vertical distance between substrate and germanene/stanene d_z, binding energy E_b, and phonon stability, of the systems of germanene/stanene supported by different 2D substrates.

Name	ICSD ID	a_{sub} (Å)	a_{sys} (Å)	a_{mis} (%)	Stacking pattern	Δ (Å)	d_z (Å)	E_b (meV Å^{-2})	Phonon stability
ZnI_2	77058	4.25	4.03	0.2	$Ge^1Ge^0I^2Zn^0I^1$	0.695	3.185	15.7	Stable
CdI_2	6066	4.24	4.11	2.2	$Ge^1Ge^0I^2Cd^0I^1$	0.672	3.182	14.8	Stable
GeI_2	23176	4.13	4.05	0.7	$Ge^1Ge^0I^2Ge^1I^2$	0.694	3.133	16.0	Stable
GaGeTe	35386	4.048	4.06	1.0	$Ge^1Ge^0Te^2Ga^1Ge^1Ge^0Ga^0Te^2$	0.698	3.028	19.4	Stable
MgI_2	52279	4.15	4.08	1.5	$Ge^1Ge^0I^2Mg^0I^1$	0.684	3.310	15.5	Stable
CuI	30363	4.25	4.06	1.0	$Ge^1Ge^0I^2Cu^1Cu^2I^1$	0.691	3.152	16.3	Stable
$CdBr_2$	31536	3.985	4.00	−0.5	$Ge^1Ge^0Br^2Cd^1Br^0$	0.695	3.166	13.7	Stable
CuBr	30091	4.096	4.02	0.0	$Ge^1Ge^0Cu^1Br^2$	0.821	1.716	162.5	Unstable
$ZrTe_2$	653213	3.952	3.99	−0.7	$Ge^1Ge^0Te^0Zr^2Te^1$	0.782	3.010	29.3	Unstable
$Y_2I_2Ga_2$	417149	4.179	4.12	2.5	$Ge^1Ge^0I^2Y^1Ga^0Ga^2Y^1I^0$	0.666	3.273	15.0	Unstable
$HfTe_2$	603713	3.910	3.97	−1.2	$Ge^1Ge^0Te^2Hf^1Te^0$	0.724	3.058	22.0	Unstable
In_3Te_4	44665	4.27	4.22	5	$Ge^1Ge^0Te^2In^0Te^1In^2Te^0In^1Te^2$	0.701	2.811	22.5	X[a]
PbI_2[b]	23762	4.56	4.61	−1.3	$Sn^1Sn^0I^2Pb^1I^0$	0.890	3.164	23.2	Stable
CaI_2[b]	52280	4.49	4.57	−2.1	$Sn^1Sn^0I^2Ca^1I^0$	0.906	3.349	22.5	Stable

[a]Fail to converge.
[b]Stanene substrates.

III. RESULTS

The overall data for the candidate substrates are listed in Tables I and II for geometric and electronic properties, respectively. Using the procedure described above, we filter out nine 2D materials from more than 185 000 entries in ICSD. Among them, seven and two candidates are suitable for germanene and stanene, respectively. All of the candidate materials can be found in the experimental literature with the experimental condition at room temperature and atmospheric pressure, and most of them are iodides. Some of them have been used as the substrate for van der Waals epitaxy (VDWE) before, for example, CdI_2 and PbI_2 [66]. Moreover, thin films of single-crystal PbI_2 with a lateral scale over tens of micrometers have been successfully synthesized very recently [67], which can serve as a planar substrate and capping layer.

From the structural parameters listed in Table I, one can find that the optimized lattice constants are almost between

the bulk lattices of the substrates and those of the freestanding germanene (4.02 Å) and stanene (4.67 Å). The majority of the most preferable stacking patterns follows a similar pattern beginning with $A^1A^0X^2$, where $A = $ Ge/Sn and X are the surface atoms of the substrate. The substrates that do not follow this rule are found to be unstable in their phonon dispersion. The $A^1A^0X^2$ stacking patterns, as described above, have tip-to-valley configurations with a much reduced interlayer distance compared to the other type of configurations. The buckling distance of germanene/stanene on substrates generally becomes smaller if the optimized system has a larger lattice constant. For germanene on substrate, 1% lattice mismatch causes roughly 1.5% change in the buckling distance, similar to and slightly larger than the value of ∼1.2% for freestanding germanene under 1% strain [68]. The vertical distance between germanene/stanene and substrates are almost all above 3 Å, and the binding energies between the layers are as small as

TABLE II. Electronic parameters, including the band gap without SOC (E_g) and with SOC ($E_{g\text{-SOC}}$), average effective mass m^*_{avg}, charge transfer q from substrate to germanene, spin expectation value s in the z direction for the VB-1 band, fitted paramters of the interaction model E_z, λ_{R1}, λ_{SO}, and $\lambda_{SO\text{-sub}}$, and M, and the Z_2 invariant of the system. Note that stanene's "Z_2" on CaI_2 is unphysical due to its semimetallic nature in this case, but becomes physical when it becomes semiconducting by, e.g., applying strain.

Name	Band gap (eV)		m^*_{avg} (m_e)		q ($|e|$)	s	E_z (V nm^{-1})	λ_{R1} (meV)	λ_{SO} (meV)	$\lambda_{SO\text{-sub}}$ (meV)	M (meV)	Z_2
	E_g	$E_{g\text{-SOC}}$	Light	Heavy								
ZnI_2	0.185	0.157	0.080	0.107	−0.022	0.994	2.7	10.8	14.0	1.1	6.2	0
CdI_2	0.158	0.132	0.069	0.095	−0.023	0.996	2.4	7.6	13.3	0.4	5.6	0
GeI_2	0.101	0.085	0.052	0.060	−0.043	0.980	1.4	10.0	8.3	−4.6	−1.3	0
GaGeTe	0.100	0.078	0.041	0.062	−0.043	1.000	1.4	0.0	11.3	−1.6	0.3	0
MgI_2	0.075	0.055	0.030	0.047	−0.031	0.998	1.1	2.5	10.3	−2.6	1.2	0
$CdBr_2$	0.018	0.004	0.014	0.023	−0.019	0.986	0.3	2.1	9.0	−3.9	1.4	0
CuI	0.002	0.006	0.018	0.018	−0.058	0.766	0.1	3.9	6.8	−6.1	1.5	1
PbI_2[a]	0.069	0.020	0.021	0.101	−0.038	0.92	0.9	19.8	31.0	−5.9	7.1	0
CaI_2[a]	0.017	Metal			−0.021	0.86	0.3	5.3	33.5	−3.3	2.9	"1"

[a]Stanene substrates.

13.7–29.3 meV Å^{-2}, which can be treated as a sign of weak vdW interaction. In contrast, the germanene-CuBr system has a small interlayer distance and large binding energy of 162.5 meV Å^{-2}, suggesting that the two materials are actually bonded.

Phonon calculations (Fig. S4 in the Suplemental Material) demonstrate that the presence of substrates only has a minor effect on the phonon dispersion of germanene and stanene, if the system is stable [48]. As shown in Fig. S4, all of the stable phonon dispersions seem to be the combination of the substrate part and the germanene/stanene part [48]. The acoustic and the Γ point out-of-plane optical (ZO) modes of the phonon dispersions of the germanene/stanene part remain nearly the same as those of the freestanding cases. Nevertheless, the existence of substrate still leads to a small shift of the in-plane longitudinal and transverse optical (LO, TO) and K point ZO frequencies, the magnitude of which generally increases with lattice mismatch (Fig. S5 [48]). The phonon dispersions of germanene on ZrTe$_2$, Y$_2$I$_2$Ga$_2$, CuBr, and HfTe$_2$ (Fig. S6) have large negative frequencies away from the Γ point and thus are marked as unstable [48]. In$_3$Te$_4$ is also categorized as an unstable substrate due to the relatively large lattice mismatch and failure of convergence in phonon dispersion calculation. However, it might be a result of the relatively lower accuracy in our choice for the parameters used in the automatic phonon calculations compared to manually fine-tuned calculations. Further calculation might be required to confirm their stability. Unless specified, we will exclude these unstable substrates in our discussion below. In addition, we have calculated the infrared (IR) activities to provide more fingerprints of the supported germanene systems (Fig. S4 [48]). The most significant peaks in all systems do not correspond to any intrinsic mode of germanene, so we believe that they come from the substrate or germanene-substrate interlayer modes.

After the structural investigation, the electronic properties, including the band structure, effective masses, charge transfer, and Z_2 topological index, are examined for the candidate systems. Let us take the germanene-CdI$_2$ system as the example again. Figure 1(g) clearly demonstrates a Dirac-cone-like band structure of germanene on CdI$_2$ with a band gap opened at the K point. Unlike the metallic germanene on MoS$_2$ [30], germanene on CdI$_2$ remains semiconducting with a gap of 0.16 eV (0.13 eV with SOC), which suggests the possibility of the fabrication of the first germanene field effect transistor (FET). The SOC split in the valence band (VB) and conduction band (CB) of germanene introduces extra effective masses, namely, the heavy hole/electron masses $m^*_{h\_h}/m^*_{e\_h}$ and light hole/electron masses $m^*_{h\_l}/m^*_{e\_l}$. While a band gap is opened, the calculated effective masses remain as small as 0.07 free electron mass m_e for light carriers. Since the intrinsic germanene is a topological insulator and has different phases under different external fields [6], it is worthy of investigation on the topological state of germanene under the influence of the substrate. The Z_2 topological index of germanene is calculated from the evolution of the Wannier charge centers (WCCs) shown in Fig. 1(i) [61]. In this case, the trajectory of the center of the largest WCC gap crosses over the WCC routes an even number of times, so the Z_2 invariant is 0. Even though the interaction between CdI$_2$ and germanene is weak,

it is large enough to be above the critical point and induce a phase transition in germanene from a topological insulator to a trivial one.

In general, germanene and stanene preserve many of their freestanding electronic properties on these substrates. As demonstrated in Fig. 2 (and Fig. S7 for a clearer view at the Fermi level around K [48]), germanene and stanene still have their Dirac-cone-like band structures on most of the candidate substrates. Notably, they become semiconducting and remain neutral on CdI$_2$, MgI$_2$, GeI$_2$, ZnI$_2$, CuI, CdBr$_2$, and GaGeTe for germanene and on PbI$_2$ for stanene, with a band gap E_g ranging from 0.002 (0.004) to 0.185 (0.157) eV for non-SOC (SOC) cases, as listed in Table II. As is known to all, the lower limit of the band gap in the channel materials of traditional FETs is around 0.4 eV. The maximum $E_{\text{g-SOC}}$ of 0.157 eV in this work is closer to such limit compared to 0.10 eV in our previous study and can be enhanced by cooperation with other gap-opening techniques, such as vertical electric field and surface adsorption, for further tunability [14,16,44]. The reason for the gap opening in germanene and stanene is the symmetry-breaking effect induced by the substrates, and the gap size is related, but not simply proportional, to the interaction strength between substrates and germanene/stanene. The corresponding tight-binding model will be discussed later to explain the phenomenon.

Although a band gap is opened, germanene (stanene) still preserves small effective masses m^* of 0.014 (0.018)–0.080 (0.107) m_e for light (heavy) carriers (Table II), where m_e denotes the mass of free electrons. Since the phonon dispersion of freestanding germanene and the supported one here are alike (Fig. S4 [48]), we assume that the relaxation time τ in our case is similar to that of the freestanding case ($\tau = 5.3$ ps). Then the carrier mobility μ of germanene on our candidate substrates estimated by $\mu = e\tau/m^*$ can be 1–9 × 10^5 cm^2 V^{-1} s^{-1} for light carriers. In comparison, the theoretical intrinsic carrier mobility of freestanding graphene and silicene are ~3 × 10^5 and ~2 × 10^5 cm^2 V^{-1} s^{-1}, respectively, without a significant band gap [19]. Note that the maximum value can exceed the intrinsic μ of germanene, because germanene on CuI and CdBr$_2$ has an even smaller band gap than freestanding germanene considering SOC. We find that $E_{\text{g-SOC}}$ and m^* of germanene on substrates have a linear relationship of $m^* \sim E_{\text{g-SOC}}/2$ [Fig. 3(a)], which is well known as the trade-off between the gap size and mobility. If such a trade-off rule is not violated at $E_{\text{g-SOC}} \sim 0.4$ eV, which is true under the tight-binding model (Fig. S10 [48]), germanene would still have a high carrier mobility over 4 × 10^4 cm^2 V^{-1} s^{-1}. As a comparison, the best carrier mobility of black phosphorus reported in experiment is on the order of 10^4 cm^2 V^{-1} s^{-1} [69], and that of MoS$_2$ is on the order of 10^3 cm^2 V^{-1} s^{-1} [70]. Impressively, germanene on CuI and stanene on CaI$_2$ have a nontrivial Z_2 topological index (see Fig. S11 for WCC evolution diagrams [48]). For stanene on CaI$_2$, although it is a semimetal [Fig. 2(i)], two groups of bands are separated by an energy "gap" near the Fermi level in the whole reciprocal space, so a topological index for the lower group of bands still can be defined [61]. Although the Z_2 index seems to be "unphysical" here, one may apply strain on the stanene/CaI$_2$ system to turn it into a semiconductor and then Z_2 will become meaningful. Considering that (1) the Z_2 index of freestanding
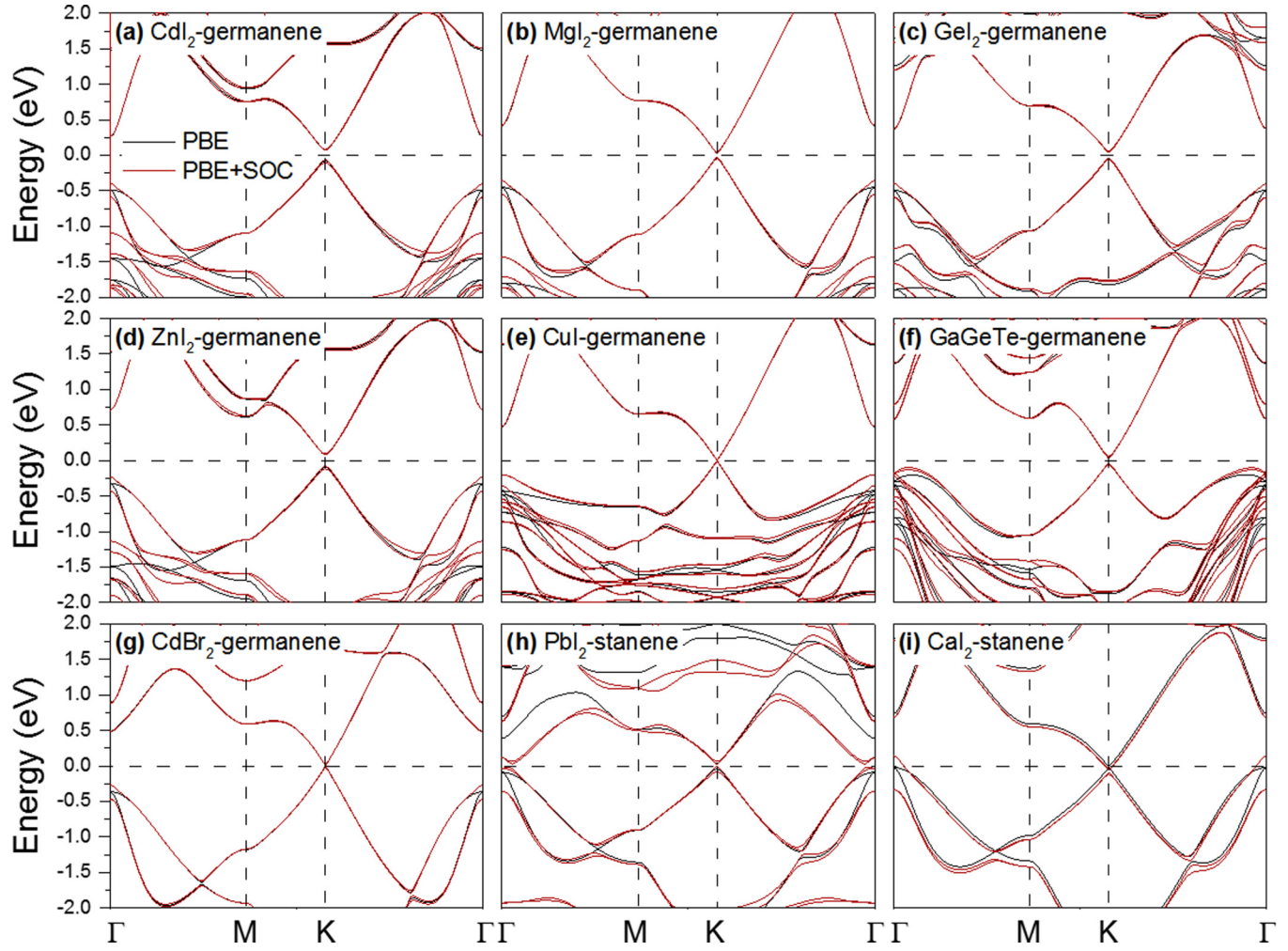
FIG. 2. (a–g) Band structures of some germanene-substrate systems with Dirac-cone-like band structures: (a) CdI$_2$, (b) MgI$_2$, (c) GeI$_2$, (d) ZnI$_2$, (e) CuI, (f) GaGeTe, and (g) CdBr$_2$. (h,i) Band structures of stanene-substrate systems with Dirac-cone-like band structures. Note that the CaI$_2$-stanene system is semiconducting without SOC, but becomes metallic when SOC is employed.

stanene does not change when the strain is between –12% and 3% [71], and (2) freestanding stanene is semiconducting when the strain is between –2% and 1% [71], CaI$_2$ supported stanene

(–2.1% strain) is likely to turn back into semiconducting while preserving the nontrivial Z_2 index when a small positive strain is applied to the system. On the rest of the substrates, where
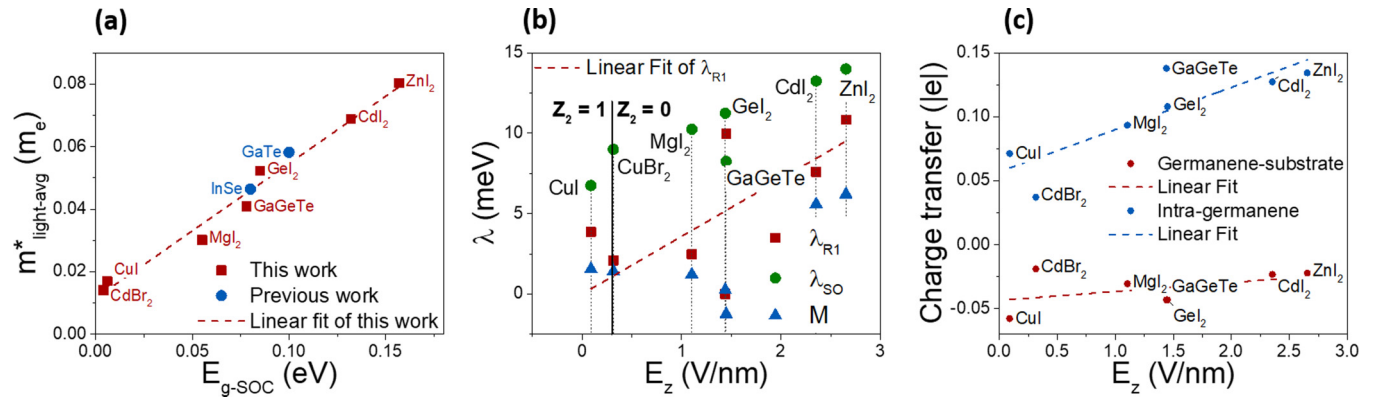

FIG. 3. (a) Relationship between the averaged light effective mass $m^*_{\text{light-avg}}$ and $E_{\text{g-SOC}}$ of germanene on different substrates. The dashed line is the linear fit of the data of this work. Some other substrates from our previous work [44] (blue dots) are also shown for comparison. (b) Relationship between E_z and the fitted λ_{SO}, $\lambda_{\text{SO-sub}}$, λ_{R1}, and M. Red dashed line is the linear fit between E_z and λ_{R1}. (c) Charge transfer q between germanene and substrate (red) and Ge atoms inside germanene (blue) as a function of E_z. Dashed lines are corresponding linear fits.

germanene and stanene open a larger band gap, they transit to band insulators, even though the interaction with the substrate is as weak as the vdW interaction.

IV. DISCUSSIONS

Here we will discuss the physical origin of the different performances of germanene/stanene on these substrates. The Hamiltonian in the vicinity of the K point of germanene/stanene under a uniform external field can be written as [6]

$$
\begin{aligned}
H_K(\vec{k}) = &\ \hbar v_F \vec{k} \cdot \vec{\tau} - \Delta E_z \tau_z + \lambda_{SO} \tau_z \sigma_z \\
&+ \tfrac{1}{2}\lambda_{R1}(\vec{\tau} \times \vec{\sigma})_z - a\lambda_{R2}\tau_z(\vec{k} \times \vec{\sigma})_z + M\sigma_z,
\end{aligned}
\tag{1}
$$

where $\vec{k}$ is the relative reciprocal vector near K. $\vec{\sigma}$ and $\vec{\tau}$ are Pauli matrices representing the spin and the A-B sublattice pseudospin in germanene/stanene, respectively. v_f is the Fermi velocity. The second term is the staggered sublattice potential term, where Δ is half of the buckling of germanene/stanene and E_z is the vertical "pseudoelectric" field applied to germanene/stanene by the substrate. $\lambda_{SO} = \lambda_{SO\text{-dirac}} + \lambda_{SO\text{-sub}}$ corresponds to the sum of the intrinsic SOC term in the Dirac material (germanene/stanene) $\lambda_{SO\text{-dirac}}$ and the SOC term induced by the substrate, $\lambda_{SO\text{-sub}}$. $\lambda_{R1} = \alpha E_z$ is the first Rashba SOC term induced by E_z. λ_{R2} is the second Rashba SOC term associated with the next-nearest-neighbor hopping. M is the "pseudomagnetic" field included to better describe the symmetry-breaking effect other than the "pseudoelectric" term [31]. This term is added because it is known that strain will induce pseudomagnetic field in graphene [72], which might apply in germanene/stanene as well. At the K point, $\vec{k} = 0$ and the λ_{R2} term vanishes, so the eigenvalues become very simple:

$$
\begin{aligned}
\varepsilon_{1,2} &= \lambda_{SO} \pm (\Delta E_z - M), \\
\varepsilon_{3,4} &= -\lambda_{SO} \pm \sqrt{(\Delta E_z + M)^2 + \lambda_{R1}^2},
\end{aligned}
\tag{2}
$$

The parameters fitted by the DFT eigenvalues are presented in Table II. Several interesting relationships can be found between them. First, λ_{R1} should be proportional to E_z in theory for freestanding graphene and germanene [73–75], which is found to be true also for supported germanene under a pseudoelectric field E_z induced by the substrate in our cases, as shown in Fig. 3(b). The fitted α in $\lambda_{R1} = \alpha E_z$ is around 0.04 Å with a Pearson's product-moment correlation coefficient r above 0.88. The inclusion of λ_{R1} changes the band gap by 0.3%–3%. The α of germanene is around two orders of magnitude larger than $\alpha \sim 6 \times 10^{-4}$ Å in silicene [6], partly due to the larger intrinsic λ_{SO} and Δ in germanene. If α becomes larger and gets closer to the value of Δ, which is possible to happen in stanene considering its even larger λ_{SO}, the correction of λ_{R1} on E_c would be significant, and the second critical electric field E_c' might be observable in practice.

Second, the charge transfer between germanene and the substrate, as well as the charge transfer between the two Ge atoms in germanene, is also proportional to E_z, as shown in Fig. 3(c). It can be understood in two ways: either the

vertical electric field E_z drives the electrons to redistribute from substrate to germanene and inside germanene, or E_z is actually a result of such charge redistribution. In any case, E_z should be linear to the charge transfer, which is confirmed by the good linear fitting displayed in Fig. 3(c).

Finally, the perfect trade-off between $E_{g\text{-SOC}}$ and the average light effective mass $m^*_{\text{light-avg}}$ shown in Fig. 3(a) can also be explained by this model. Using the Fermi velocity of freestanding germanene $v_f = 8.8 \times 10^5$ m s^{-1} [76], we calculate the reciprocal for the second-order derivative of the bands at the K point, $1/E_{kx}'' \equiv [\partial^2 E(k_x, k_y, E_z)/\partial k_x^2]^{-1}|_{k_x=k_y=0}$ under the assumption of $M = \lambda_{R2} = 0$ and $\lambda_{R1} = 0.04E_z$ (Fig. S10 [48]). Since $m^*_{K\Gamma} \propto 1/E_{kx}''$, Fig. S10 can also demonstrate the relationship between $m^*_{K\Gamma}$ and $E_{g\text{-SOC}}$ [48]. The average light effective mass is almost perfectly proportional to $E_{g\text{-SOC}}$ when $E_{g\text{-SOC}} < 0.4$ eV. Note that germanene on all suitable substrates in this work satisfies the condition. All of the correlations found above can be viewed as a cross validation for the correctness of the model and support the opinion that the different behaviors of germanene on substrates are the result of the external fields, mainly electric field, applied by the substrate.

Note that the PBE functional usually underestimates the band-gap size, which can be improved by using hybrid functionals like HSE06 [77–79]. However, we do not expect that such replacement would affect the above general conclusion for suitable substrates, because we previously found that using HSE06 only enlarges the gap size by ∼30% compared to the PBE functional without SOC and does not change the shape of the Dirac cone for germanene on suitable substrates [44]. Moreover, the SOC effect will almost cancel such an increase of band gap in germanene [44], so the HSE06 + SOC band gap might be similar to the PBE band gap without SOC in germanene. For example, the band gaps of germanene on GaTe and InSe are 0.12, 0.10, and 0.16 eV and 0.11, 0.08, and 0.14 eV, respectively, for PBE, PBE+SOC, and HSE06 calculations [44]. We have performed the HSE06 calculation of germanene on CuI as a test with a k grid of $3 \times 3 \times 1$ and the identical q grid (Fig. S18 [48]). The band gap predicted by HSE06 at the K point is 10 meV, similar to the value of PBE + SOC (6 meV). Hence we believe that using the HSE06 functional would not have significant impact on our conclusions about the selection of suitable substrates.

The change of the band gap size by using a hybrid functional may also lead to a different Z_2 invariant [40,80]. However, it does not matter for most substrates found in this work, on which germanene is predicted to have even Z_2, since germanene is more likely to be topologically trivial with a larger band gap. On CuI, germanene is predicted to have odd Z_2 on the PBE level. There is the possibility that the result would be different by using a different functional, but the band gap given by HSE06 is only 10 meV, which is still within the possible range of the topologically nontrivial phase (∼23 meV) [9].

We have made several additional investigations on the stability of germanene supported by CuI. First, we have performed molecular dynamics (MD) simulation for a 3×3 germanene-CuI supercell with an initial temperature of 800 K for about 2 ps (see the caption of Fig. S12 for computational details [48]). The hexagonal structure of germanene on CuI is

almost preserved after 2 ps (Fig. S12 [48]). There is oscillation in the buckling of germanene, but the buckled structure is generally preserved (Fig. S13 [48]). Notably, such oscillation for germanene on CuI seems to be smaller than the case without CuI (Fig. S13 [48]), implying that CuI might help stabilize germanene in the vertical direction. Second, a 1×1 unit cell might enforce the system to fake stability. We have performed geometry optimization for the 5×5 supercell of germanene on CuI (Fig. S15) and found no significant change in the geometry of germanene and CuI [48].

In this work, we focused on candidate substrates that can form 1×1 stacking patterns with our target materials, germanene and stanene. It is possible for germanene and stanene to take a supercell other than 1×1 on substrates. In theory, a large coincident lattice with rotations can be used for 2D crystals with different lattice constants to achieve very small mismatch, around 1% [81]. However, such coincident lattice is not used in this work due to the following reasons. (1) Such a coincident lattice does not necessarily represent the real configuration in experiment, even if it has very small mismatch, below 1%. For example, germanene on MoS_2 takes the nonrotated 5×5 supercell on 6×6 MoS_2 with 5% strain [30], instead of the $27.8°$ rotated configuration with 0.7% strain proposed in theory [31]. This may be because germanene is somehow flexible in its planar lattice constant due to its buckled geometry. Considering the large lattice mismatch of germanene and MoS_2, we believe it is more likely for germanene to take nonrotated configurations on substrates with <6% lattice mismatch in our case. (2) We have performed the calculation of $\sqrt{21} \times \sqrt{21}$ R 72.656 germanene on $\sqrt{19} \times \sqrt{19}$ CuI. The lattice mismatch is 0.4%. The result of geometry optimization and band structure shows features very similar to the 1×1 stacking case (Fig. S17 [48]), so CuI is still a suitable substrate for germanene with such rotated cell. We believe that the suitable substrates found in our work will still be suitable using the rotated coincident lattice. In addition, our methodology can be easily extended to take into account those substrates with incommensurate lattice constants compared to the target material (germanene and stanene in our case). Since computations on such coincident lattices with rotation are quite time consuming, extensive investigations remain as a future task.

In addition to being the substrate guide for experimentalists, our research might lead to at least two types of future study. First, one can make a vertical heterojunction, i.e., sandwiched germanene/stanene between different types of substrates, to tune their electronic properties and protect them from the ambient environment. The pseudoelectric fields from the effect of the two capping layers may either cancel or enhance with

each other. If germanene is sandwiched between two substrates similar to ZnI_2 that have $E_z \sim 2.5\,\mathrm{V\,nm^{-1}}$ with an enhanced effect, it is possible to double the band gap in germanene to ~0.4 eV to make it suitable for FET application. In contrast, two substrates with a canceled effect may lead to small or zero electric field, resulting in a nontrivial Z_2 invariant in germanene. Second, it is interesting to put germanene on the junction of two types of the substrates, say CuI and ZnI_2, to see whether it will have the topological edge state in germanene/stanene at the boundary of two substrates (or "topological domain wall" [10]). Note that in such a system, germanene can be intact without any geometric boundary.

V. CONCLUSIONS

We have found several suitable 2D substrate candidates, including some of the CdI_2-type materials, CuI, and GaGeTe, for germanene and stanene by using the combination of density functional theory and materials informatics. We have succeeded in finding more candidates than previous manual searches, and some of them show better performance than those previously found. The suitable substrates can preserve the quasifreestanding geometry and the Dirac-cone-like band structure of germanene and stanene with a band gap of 0.004–0.157 eV opened at the Dirac point. Germanene on CuI and stanene on CaI_2 are found to have odd Z_2 invariant, and the former one is a topological insulator. In addition, we have found that the interaction between germanene and the substrates can be well described by the tight-binding Hamiltonian of germanene under uniform external fields. The analysis using the Hamiltonian shows that suitable substrates mainly act like a "pseudoelectric" field on germanene, whose field strength dominates the band gap and topological phase of germanene. The linear trade-off between the band gap and the average light effective mass can be well reproduced when the band gap is below 0.4 eV. The fitted extrinsic Rashba coefficient is found to be almost linear to the "pseudoelectric" field, similar to its behavior under real electric field. We hope our research can shed light on the first synthesis of germanene and stanene with semiconducting Dirac-cone-like band structure and open up alternative areas of research for them.

ACKNOWLEDGMENTS

[1] A. K. Geim and K. S. Novoselov, Nat. Mater. **6**, 183 (2007).

[2] C. L. Kane and E. J. Mele, Phys. Rev. Lett. **95**, 226801 (2005).

[3] R. F. Service, Science **348**, 490 (2015).

[4] A. Molle, J. Goldberger, M. Houssa, Y. Xu, S.-C. Zhang, and D. Akinwande, Nat. Mater. **16**, 163 (2017).

[5] S. Cahangirov, M. Topsakal, E. Aktürk, H. Šahin, and S. Ciraci, Phys. Rev. Lett. **102**, 236804 (2009).

[6] M. Ezawa, Phys. Rev. Lett. **109**, 055502 (2012).

[7] Y. Xu, B. Yan, H.-J. Zhang, J. Wang, G. Xu, P. Tang, W. Duan, and S.-C. Zhang, Phys. Rev. Lett. **111**, 136804 (2013).

[8] Y. Wang, Z. Ni, Q. Liu, R. Quhe, J. Zheng, M. Ye, D. Yu, J. Shi, J. Yang, J. Li, and J. Lu, Adv. Funct. Mater. **25**, 68 (2015).

[9] C. C. Liu, W. Feng, and Y. Yao, Phys. Rev. Lett. **107**, 076802 (2011).

[10] M. Wang, L. Liu, C.-C. C. Liu, and Y. Yao, Phys. Rev. B **93**, 155412 (2016).

[11] Y. Yao, F. Ye, X. L. Qi, S. C. Zhang, and Z. Fang, Phys. Rev. B **75**, 041401 (2007).

[12] J. E. Moore, Nature **464**, 194 (2010).

[13] M. Ezawa, J. Supercond. Novel Magn. **28**, 1249 (2015).

[14] Z. Ni, Q. Liu, K. Tang, J. Zheng, J. Zhou, R. Qin, Z. Gao, D. Yu, and J. Lu, Nano Lett. **12**, 113 (2012).

[15] Z. Ni, H. Zhong, X. Jiang, R. Quhe, G. Luo, Y. Wang, M. Ye, J. Yang, J. Shi, and J. Lu, Nanoscale **6**, 7609 (2014).

[16] M. Ye, R. Quhe, J. Zheng, Z. Ni, Y. Wang, Y. Yuan, G. Tse, J. Shi, Z. Gao, and J. Lu, Phys. E (Amsterdam, Neth.) **59**, 60 (2014).

[17] N. D. Drummond, V. Zólyomi, and V. I. Fal'Ko, Phys. Rev. B **85**, 075423 (2012).

[18] M. Ezawa, New J. Phys. **14**, 033003 (2012).

[19] X.-S. Ye, Z.-G. Shao, H. Zhao, L. Yang, and C.-L. Wang, RSC Adv. **4**, 21216 (2014).

[20] J.-A. Yan, R. Stein, D. M. Schaefer, X.-Q. Wang, and M. Y. Chou, Phys. Rev. B **88**, 121403 (2013).

[21] B. Bishnoi and B. Ghosh, RSC Adv. **3**, 26153 (2013).

[22] A. J. Mannix, B. Kiraly, M. C. Hersam, and N. P. Guisinger, Nat. Rev. Chem. **1**, 14 (2017).

[23] L. Li, S. Z. Lu, J. Pan, Z. Qin, Y. Wang, Y. Wang, G. Cao, S. Du, and H. Gao, Adv. Mater. **26**, 4820 (2014).

[24] A. Acun, L. Zhang, P. Bampoulis, M. Farmanbar, A. van Houselt, A. N. Rudenko, M. Lingenfelder, G. Brocks, B. Poelsema, M. I. Katsnelson, and H. J. W. Zandvliet, J. Phys.: Condens. Matter **27**, 443002 (2015).

[25] M. E. Dávila, L. Xian, S. Cahangirov, A. Rubio, and G. Le Lay, New J. Phys. **16**, 095002 (2014).

[26] P. Bampoulis, L. Zhang, A. Safaei, R. van Gastel, B. Poelsema, and H. J. W. Zandvliet, J. Phys.: Condens. Matter **26**, 442001 (2014).

[27] L. Zhang, P. Bampoulis, A. van Houselt, and H. J. W. Zandvliet, Appl. Phys. Lett. **107**, 111605 (2015).

[28] M. Derivaz, D. Dentel, R. Stephan, M.-C. Hanf, A. Mehdaoui, P. Sonnet, and C. Pirri, Nano Lett. **15**, 2510 (2015).

[29] F. Zhu, W. Chen, Y. Xu, C. Gao, D. Guan, C. Liu, D. Qian, S.-C. Zhang, and J. Jia, Nat. Mater. **14**, 1020 (2015).

[30] L. Zhang, P. Bampoulis, A. N. Rudenko, Q. Yao, A. van Houselt, B. Poelsema, M. I. Katsnelson, and H. J. W. Zandvliet, Phys. Rev. Lett. **116**, 256804 (2016).

[31] T. Amlaki, M. Bokdam, and P. J. Kelly, Phys. Rev. Lett. **116**, 256805 (2016).

[32] C.-C. Ren, Y. Feng, S.-F. Zhang, C.-W. Zhang, and P.-J. Wang, RSC Adv. **7**, 9176 (2017).

[33] W. Xiong, C. Xia, J. Du, T. Wang, Y. Peng, Z. Wei, and J. Li, Nanotechnology **28**, 195702 (2017).

[34] T. P. Kaloni and U. Schwingenschlögl, J. Appl. Phys. **114**, 184307 (2013).

[35] S. Kokott, L. Matthes, and F. Bechstedt, Phys. Status Solidi RRL **7**, 538 (2013).

[36] F. Matusalem, F. Bechstedt, M. Marques, and L. K. Teles, Phys. Rev. B **94**, 241403 (2016).

[37] H. Wang, S. T. Pi, J. Kim, Z. Wang, H. H. Fu, and R. Q. Wu, Phys. Rev. B **94**, 035112 (2016).

[38] Y. Ding and Y. Wang, J. Phys. Chem. C **119**, 27848 (2015).

[39] Y. Fang, Z.-Q. Huang, C.-H. Hsu, X. Li, Y. Xu, Y. Zhou, S. Wu, F.-C. Chuang, and Z.-Z. Zhu, Sci. Rep. **5**, 14196 (2015).

[40] L. Matthes, S. Küfner, J. Furthmüller, and F. Bechstedt, Phys. Rev. B **94**, 085410 (2016).

[41] L. Matthes, S. Küfner, J. Furthmüller, and F. Bechstedt, Phys. Rev. B **93**, 121106 (2016).

[42] W. J. Yu, Y. Liu, H. Zhou, A. Yin, Z. Li, Y. Huang, and X. Duan, Nat. Nanotechnol. **8**, 952 (2013).

[43] L. Britnell, R. V. Gorbachev, R. Jalil, B. D. Belle, F. Schedin, A. Mishchenko, T. Georgiou, M. I. Katsnelson, L. Eaves, S. V. Morozov, N. M. R. Peres, J. Leist, A. K. Geim, K. S. Novoselov, and L. A. Ponomarenko, Science **335**, 947 (2012).

[44] Z. Ni, E. Minamitani, Y. Ando, and S. Watanabe, Phys. Chem. Chem. Phys. **17**, 19039 (2015).

[45] A. Belsky, M. Hellenbrandt, V. L. Karen, and P. Luksch, Acta Crystallogr., Sect. B: Struct. Sci. **58**, 364 (2002).

[46] Z. Otwinowski and W. Minor, *International Tables for Crystallography Volume G: Definition and Exchange of Crystallographic Data First Online Edition (2006)* (International Union of Crystallography, Chester, UK, 2006).

[47] S. Lebègue, T. Björkman, M. Klintenberg, R. M. Nieminen, and O. Eriksson, Phys. Rev. X **3**, 031002 (2013).

[48] See Supplemental Material at http://link.aps.org/supplemental/10.1103/PhysRevB.96.075427 for the bulk structure of suitable substrates; lattice constant optimization, stacking pattern, phonon dispersion, IR activity, band structure in detail, and WCC evolution of supported germanene and stanene; band gap given by hybrid functional, molecular dynamics simulation, and investigation of large rotated commensurate supercell of germanen on CuI; test for norm-conserving pseudopotentials; tight binding analysis about pseudoelectric field and effective mass; investigation of selection criterion of layered materials.

[49] P. Giannozzi, S. Baroni, N. Bonini, M. Calandra, R. Car, C. Cavazzoni, D. Ceresoli, G. L. Chiarotti, M. Cococcioni, I. Dabo, A. Dal Corso, S. de Gironcoli, S. Fabris, G. Fratesi, R. Gebauer, U. Gerstmann, C. Gougoussis, A. Kokalj, M. Lazzeri, L. Martin-Samos *et al.*, J. Phys.: Condens. Matter **21**, 395502 (2009).

[50] G. Kresse and D. Joubert, Phys. Rev. B **59**, 1758 (1999).

[51] A. Dal Corso, Comput. Mater. Sci. **95**, 337 (2014).

[52] M. Dion, H. Rydberg, E. Schröder, D. C. Langreth, and B. I. Lundqvist, Phys. Rev. Lett. **92**, 246401 (2004).

[53] J. Klime, D. R. Bowler, A. Michaelides, J. Klimeš, D. R. Bowler, and A. Michaelides, Phys. Rev. B **83**, 195131 (2011).

[54] T. Thonhauser, V. R. Cooper, S. Li, A. Puzder, P. Hyldgaard, and D. C. Langreth, Phys. Rev. B **76**, 125112 (2007).

[55] G. Román-Pérez and J. M. Soler, Phys. Rev. Lett. **103**, 096102 (2009).

[56] J. P. Perdew, K. Burke, and M. Ernzerhof, Phys. Rev. Lett. **77**, 3865 (1996).

[57] J. D. Pack and H. J. Monkhorst, Phys. Rev. B **16**, 1748 (1977).

[58] L. Bengtsson, Phys. Rev. B **59**, 12301 (1999).

[59] D. R. Hamann, Phys. Rev. B **88**, 085117 (2013).

[60] M. Schlipf and F. Gygi, Comput. Phys. Commun. **196**, 36 (2015).

[61] A. A. Soluyanov and D. Vanderbilt, Phys. Rev. B **83**, 235401 (2011).

[62] A. A. Mostofi, J. R. Yates, Y. S. Lee, I. Souza, D. Vanderbilt, and N. Marzari, Comput. Phys. Commun. **178**, 685 (2008).

[63] A. A. Mostofi, J. R. Yates, G. Pizzi, Y.-S. Lee, I. Souza, D. Vanderbilt, and N. Marzari, Comput. Phys. Commun. **185**, 2309 (2014).

[64] E. Scalise, M. Houssa, G. Pourtois, B. van den Broek, V. Afanas'ev, and A. Stesmans, Nano Res. **6**, 19 (2013).

[65] L.-F. Huang, P.-L. Gong, and Z. Zeng, Phys. Rev. B **91**, 205433 (2015).

[66] S. Takeyama, K. Watanabe, M. Ichihara, K. Suzuki, and N. Miura, J. Appl. Phys. **68**, 2735 (1990).

[67] Y. Wang, Y.-Y. Sun, S. Zhang, T.-M. Lu, and J. Shi, Appl. Phys. Lett. **108**, 013105 (2016).

[68] J.-A. Yan, S.-P. Gao, R. Stein, and G. Coard, Phys. Rev. B **91**, 245403 (2015).

[69] J. Qiao, X. Kong, Z.-X. Hu, F. Yang, and W. Ji, Nat. Commun. **5**, 4475 (2014).

[70] H. S. Lee, S. S. Baik, K. Lee, S. Min, P. J. Jeon, J. S. Kim, K. Choi, H. J. Choi, J. H. Kim, and S. Im, ACS Nano **9**, 8312 (2015).

[71] Z. Q. Huang, C. H. Hsu, F. C. Chuang, Y. T. Liu, H. Lin, W. S. Su, V. Ozolins, and A. Bansil, New J. Phys. **16**, 105018 (2014).

[72] N. Levy, S. A. Burke, K. L. Meaker, M. Panlasigui, A. Zettl, F. Guinea, A. H. C. Neto, and M. F. Crommie, Science **329**, 544 (2010).

[73] W.-K. Tse, Z. Qiao, Y. Yao, A. H. MacDonald, and Q. Niu, Phys. Rev. B **83**, 155447 (2011).

[74] D. N. Sheng, Z. Y. Weng, L. Sheng, and F. D. M. Haldane, Phys. Rev. Lett. **97**, 036808 (2006).

[75] H. Min, J. E. Hill, N. A. Sinitsyn, B. R. Sahu, L. Kleinman, and A. H. MacDonald, Phys. Rev. B **74**, 165310 (2006).

[76] S. Trivedi, A. Srivastava, and R. Kurchania, J. Comput. Theor. Nanosci. **11**, 781 (2014).

[77] J. Heyd, G. E. Scuseria, and M. Ernzerhof, J. Chem. Phys. **118**, 8207 (2003).

[78] J. Heyd and G. E. Scuseria, J. Chem. Phys. **121**, 1187 (2004).

[79] J. Heyd, G. E. Scuseria, and M. Ernzerhof, J. Chem. Phys. **124**, 219906 (2006).

[80] C. Si, J. Liu, Y. Xu, J. Wu, B. L. Gu, and W. Duan, Phys. Rev. B **89**, 115429 (2014).

[81] D. S. Koda, F. Bechstedt, M. Marques, and L. K. Teles, J. Phys. Chem. C **120**, 10895 (2016).